# Multipolar second harmonic generation from planar arrays of Au nanoparticles

**Antonio Capretti,[1,2,3] Gary F. Walsh,[1,4] Salvatore Minissale,[1] Jacob Trevino,[1,5] Carlo Forestiere,[1] Giovanni Miano,[2] and Luca Dal Negro[1,5,*]**

[1]*Department of Electrical and Computer Engineering and Photonics Center, Boston University, 8 Saint Mary's Street, Boston, Massachusetts 02215 USA*
[2]*Department of Electrical Engineering, Università degli Studi di Napoli Federico II, Via Claudio 21, Napoli 80125, Italy*
[3]*CNR-SPIN, Complesso Universitario di Monte S. Angelo, Via Cintia, Napoli 80126, Italy*
[4]*US Army NSRDEC, Nanomaterials Science Team, Kansas Street, Natick, Massachusetts 01760 USA*
[5]*Division of Materials Science and Engineering, Boston University, 15 Saint Mary's Street, Brookline, Massachusetts 02446 USA*
[*]*dalnegro@bu.edu*

**Abstract:** We demonstrate optical Second Harmonic Generation (SHG) in planar arrays of cylindrical Au nanoparticles arranged in periodic and deterministic aperiodic geometries. In order to understand the respective roles of near-field plasmonic coupling and long-range photonic interactions on the SHG signal, we systematically vary the interparticle separation from 60 nm to distances comparable to the incident pump wavelength. Using polarization-resolved measurements under femtosecond pumping, we demonstrate multipolar SHG signal largely tunable by the array geometry. Moreover, we show that the SHG signal intensity is maximized by arranging Au nanoparticles in aperiodic spiral arrays. The possibility to engineer multipolar SHG in planar arrays of metallic nanoparticles paves the way to the development of novel optical elements for nanophotonics, such as nonlinear optical sensors, compact frequency converters, optical mixers, and broadband harmonic generators on a chip.

**OCIS codes:** (190.0190) Nonlinear optics; (260.3910) Metal optics; (310.6628) Subwavelength structures, nanostructures.

## References and links

1. E. Fort and S. Gresillon, "Surface enhanced fluorescence," J. Phys. D Appl. Phys. **41**(1), 013001 (2008).
2. P. L. Stiles, J. A. Dieringer, N. C. Shah, and R. P. Van Duyne, "Surface-enhanced Raman spectroscopy," Annu Rev Anal Chem (Palo Alto Calif) **1**(1), 601–626 (2008).
3. C. K. Chen, T. F. Heinz, D. Ricard, and Y. R. Shen, "Surface-enhanced second-harmonic generation and Raman scattering," Phys. Rev. B **27**(4), 1965–1979 (1983).
4. G. T. Boyd, Z. H. Yu, and Y. R. Shen, "Photoinduced luminescence from the noble metals and its enhancement on roughened surfaces," Phys. Rev. B Condens. Matter **33**(12), 7923–7936 (1986).
5. W. L. Barnes, A. Dereux, and T. W. Ebbesen, "Surface plasmon subwavelength optics," Nature **424**(6950), 824–830 (2003).
6. S. A. Maier, *Plasmonics: fundamentals and applications* (Springer, 2007).
7. F. Hache, D. Ricard, C. Flytzanis, and U. Kreibig, "The optical Kerr effect in small metal particles and metal colloids: the case of gold," Appl. Phys., A Mater. Sci. Process. **47**(4), 347–357 (1988).
8. C. K. Chen, A. R. B. de Castro, and Y. R. Shen, "Surface-enhanced second-harmonic generation," Phys. Rev. Lett. **46**(2), 145–148 (1981).
9. G. S. Agarwal and S. S. Jha, "Theory of second harmonic generation at a metal surface with surface plasmon excitation," Solid State Commun. **41**(6), 499–501 (1982).
10. is J. I. Dadap, J. Shan, K. B. Eisenthal, and T. F. Heinz, "Second-harmonic Rayleigh scattering from a sphere of centrosymmetric material," Phys. Rev. Lett. **83**(20), 4045–4048 (1999).
11. P. Guyot-Sionnest, W. Chen, and Y. R. Shen, "General considerations on optical second-harmonic generation from surfaces and interfaces," Phys. Rev. B Condens. Matter **33**(12), 8254–8263 (1986).
12. P. Guyot-Sionnest and Y. R. Shen, "Local and nonlocal surface nonlinearities for surface optical second-harmonic generation," Phys. Rev. B Condens. Matter **35**(9), 4420–4426 (1987).
13. B. Lamprecht, A. Leitner, and F. R. Aussenegg, "SHG studies of plasmon dephasing in nanoparticles," Appl. Phys. B **68**(3), 419–423 (1999).

14. B. K. Canfield, S. Kujala, K. Jefimovs, T. Vallius, J. Turunen, and M. Kauranen, "Polarization effects in the linear and nonlinear optical responses of gold nanoparticle arrays," J. Opt. A, Pure Appl. Opt. **7**(2), S110–S117 (2005).
15. M. D. McMahon, R. Lopez, and R. F. Jr. Haglund, E. A. Ray, and P. H. Bunton, "Second-harmonic generation from arrays of symmetric gold nanoparticles," Phys. Rev. B **73**(4), 041401 (2006).
16. M. D. McMahon, D. Ferrara, C. T. Bowie, R. Lopez, and R. F. Haglund, Jr, "Second harmonic generation from resonantly excited arrays of gold nanoparticles," Appl. Phys. B **87**(2), 259–265 (2007).
17. C. Awada, F. Kessi, Ch. Jonin, P. M. Adam, S. Kostcheev, R. Bachelot, P. Royer, I. Russier-Antoine, E. Benichou, G. Bachelier, and P.-F. Brevet, "On- and off-axis second harmonic generation from an array of gold metallic nanocylinders," J. Appl. Phys. **110**(2), 023109 (2011).
18. B. K. Canfield, H. Husu, J. Laukkanen, B. Bai, M. Kuittinen, J. Turunen, and M. Kauranen, "Local field asymmetry drives second-harmonic generation in non-centrosymmetric nanodimers," Nano Lett. **7**(5), 1251–1255 (2007).
19. R. Boyd, *Nonlinear optics* (Academic Press, 2003).
20. M. Breit, V. A. Podolskiy, S. Gresillon, G. von Plessen, J. Feldmann, J. C. Rivoal, P. Gadenne, A. K. Sarychev, and V. M. Shalaev, "Experimental observation of percolation-enhanced nonlinear light scattering from semicontinuous metal films," Phys. Rev. B **64**(12), 125106 (2001).
21. R. Dallapiccola, A. Gopinath, F. Stellacci, and L. Dal Negro, "Quasi-periodic distribution of plasmon modes in two-dimensional Fibonacci arrays of metal nanoparticles," Opt. Express **16**(8), 5544–5555 (2008).
22. L. Dal Negro, N.-N. Feng, and A. Gopinath, "Electromagnetic coupling and plasmon localization in deterministic aperiodic arrays," J. Opt. A, Pure Appl. Opt. **10**(6), 064013 (2008).
23. A. Gopinath, S. V. Boriskina, N.-N. Feng, B. M. Reinhard, and L. Dal Negro, "Photonic-plasmonic scattering resonances in deterministic aperiodic structures," Nano Lett. **8**(8), 2423–2431 (2008).
24. L. Dal Negro and S. V. Boriskina, "Deterministic aperiodic nanostructures for photonics and plasmonics applications," Laser. Photon. Rev. **6**(2), 178–218 (2012).
25. J. Trevino, H. Cao, and L. Dal Negro, "Circularly symmetric light scattering from nanoplasmonic spirals," Nano Lett. **11**(5), 2008–2016 (2011).
26. J. Trevino, S. F. Liew, H. Noh, H. Cao, and L. Dal Negro, "Geometrical structure, multifractal spectra and localized optical modes of aperiodic Vogel spirals," Opt. Express **20**(3), 3015–3033 (2012).
27. S. F. Liew, H. Noh, J. Trevino, L. D. Negro, and H. Cao, "Localized photonic bandedge modes and orbital angular momenta of light in a golden-angle spiral," Opt. Express **19**(24), 23631–23642 (2011).
28. A. Doicu, T. Wriedt, and Y. Eremin, *Light scattering by system of particles* (Springer-Verlag, 2006).
29. C. Forestiere, G. Iadarola, L. Dal Negro, and G. Miano, "Near field calculation based on the T-matrix method with discrete sources," J. Quant. Spectrosc. Radiat. Transf. **112**(14), 2384–2394 (2011).
30. H. Raether, *Surface Plasmons on Smooth and Rough Surfaces and on Gratings* (Springer-Verlag, 1988), Chap. 6.
31. G. D'Aguanno, N. Mattiucci, M. J. Bloemer, D. de Ceglia, M. A. Vincenti, and A. Alù, "Transmission resonances in plasmonic metallic gratings," J. Opt. Soc. Am. B **28**(2), 253–264 (2011).
32. J. Nappa, G. Revillod, I. Russier-Antoine, E. Benichou, C. Jonin, and P.-F. Brevet, "Electric dipole origin of the second harmonic generation of small metallic particles," Phys. Rev. B **71**(16), 165407 (2005).
33. G. Bachelier, I. Russier-Antoine, E. Benichou, C. Jonin, and P.-F. Brevet, "Multipolar second-harmonic generation in noble metal nanoparticles," J. Opt. Soc. Am. B **25**(6), 955–960 (2008).
34. J. Butet, G. Bachelier, I. Russier-Antoine, C. Jonin, E. Benichou, and P.-F. Brevet, "Interference between selected dipoles and octupoles in the optical second-harmonic generation from spherical gold nanoparticles," Phys. Rev. Lett. **105**(7), 077401 (2010).
35. J. Butet, I. Russier-Antoine, C. Jonin, N. Lascoux, E. Benichou, and P.-F. Brevet, "Sensing with multipolar second harmonic generation from spherical metallic nanoparticles," Nano Lett. **12**(3), 1697–1701 (2012).
36. S. Kujala, B. K. Canfield, M. Kauranen, Y. Svirko, and J. Turunen, "Multipole interference in the second-harmonic optical radiation from gold nanoparticles," Phys. Rev. Lett. **98**(16), 167403 (2007).
37. Y. L. Xu, "Electromagnetic scattering by an aggregate of spheres," Appl. Opt. **34**(21), 4573–4588 (1995).

## 1. Introduction

Metal nanoparticles (NPs) have been employed for decades to enhance the efficiency of optical processes, including Raman scattering, fluorescence, and multiphoton absorption because they support Localized Surface Plasmons (LSPs), which are collective electron oscillations bound to the particle surface [1–4]. When plasmons are resonantly excited, the incident electromagnetic field is significantly enhanced in the metallic NPs [5,6]. This enables strong nonlinear optical effects at relatively low excitation powers, such as harmonic generation and the Kerr effect [7,8]. In particular, second harmonic generation (SHG) is a nonlinear optical process in which a medium excited by two photons at a fundamental (*i.e.*, pump) frequency $\omega_0$ emits one photon at twice that frequency $2\omega_0$. Second harmonic generation from NPs arises from two contributions, a bulk source and a surface one. In noble metal NPs the local bulk source is absent because of the material centrosymmetry, and only the non-local contribution exists. The local surface contribution to SHG is due to the

symmetry breaking at the interface with the embedding medium [9,10]. The relative magnitudes of the non-local bulk and local surface SHG contributions depend generally on the shape of the nanoparticles and on the optical properties of the metal at the fundamental and SHG wavelengths [11,12].

In the last few years, SHG from planar arrays of metal NPs has been investigated for a variety of NP shapes, sizes, and under different excitation-collection and polarization conditions [13–18]. In order to maximize the intensity of the SHG from a planar array, the particle shape, the interparticle separations and the array geometry must be designed to excite LSPs at the fundamental wavelength, producing strong near-field enhancement. This is due to the fact that the intensity of the SHG signal grows with the square of the intensity of the local electric field at the pump wavelength. In addition, the particle shape plays a fundamental role due to symmetry selection rules governing the SHG [19]. For example, L-shaped NPs have been specifically studied to remove single particle centrosymmetry. In this case the linear and nonlinear optical behavior is strongly dependent on the polarization state of the excitation [13,14]. In 1999 Lamprecht et al. demonstrated that the SHG signal from arrays of L-shaped particles can be greatly increased if the particles are oriented in such a way that the overall array becomes non-centrosymmetric [13]. Canfield et al. investigated SHG from non-centrosymmetric NPs dimers, demonstrating that the asymmetry of the local electric field distribution over the entire array plays a role in SHG as important as the enhancement of the near-field intensity by the NPs [18]. Angularly resolved studies of the SHG from discontinuous metal percolation films also featured strong peaks of second harmonic signal in the direction of specular reflection as well as a diffuse scattering background [20]. However, the role of the planar array geometry on the SHG from metallic NPs is not yet fully understood.

Deterministic aperiodic nanostructures (DANS) have been shown to exhibit distinctive scattering properties associated to the increased localization of photonic-plasmonic modes, such as broadband scattering resonances, enhanced near-field intensities, largely controllable angular scattering, enhanced colorimetric responses and Raman cross sections employed for biosensing applications [21–24]. Recently, DANS lacking both translational and rotational symmetry, consisting of aperiodic Vogel spirals of metallic NPs, have also been demonstrated to exhibit polarization-insensitive planar light diffraction and distinctive photonic modes carrying discrete values of optical angular momentum [25–27].

In this work, we investigate the role of the array geometry on the intensity and on the polarization properties of the SHG from metallic nano-cylinders arranged in planar structures of progressively increasing complexity. In particular we focus on periodic, quasi-periodic Fibonacci and aperiodic Golden Angle (GA) spiral arrays in the nonlinear optical regime. Detailed studies on the Fibonacci and GA spiral geometries as well as their linear scattering properties have been discussed elsewhere [21–27].

## 2. Array design and fabrication

We investigate SHG in periodic, Fibonacci and GA spiral arrays of cylindrical gold nanoparticles with a height of 30 nm and a diameter of 200 nm. The dimensions of the gold nanocylinders have been chosen in such a way that the peak of the scattered pump signal is overlapping the pump wavelength (*i.e.*, 780 nm) in the absence of interactions among cylinders. The T-matrix numerical method has been employed for electromagnetic scattering calculations [28,29], assuming a perfect cylindrical shape.

We fabricate a set of samples on a transparent fused silica substrate by electron beam lithography (EBL). For each sample, a 180 nm thick PMMA (poly(methyl methacrylate)) film is first spin-coated onto the substrate, and then soft-baked at 180°C for 20 minutes. The PMMA film is nanopatterned by EBL (using a Zeiss SUPRA 40VP SEM equipped with Raith beam blanker and NPGS) and developed in MIBK:IPA (1:3). A 2 nm Cr adhesion layer and a 30 nm gold layer are deposited over the PMMA film by electron beam evaporation. Finally the sample is immersed in heated acetone for the lift-off process.

Each array has a circular shape with a diameter of 50 µm. In order to explore both the short-range plasmonic and long-range photonic coupling regimes we consider arrays with edge-to-edge interparticle separations $L$ ranging from 60 nm to 650 nm. For periodic and Fibonacci arrays the interparticle separation is defined as the minimum edge-to-edge particle separation, while for the GA spirals it is defined as the average nearest neighbor edge-to-edge separation, as discussed by Trevino et. al. [25,26]. In Fig. 1 we show the Scanning Electron Micrographs (SEM) of periodic (a), Fibonacci (b) and GA spiral (c) arrays with an interparticle separation of 60 nm.
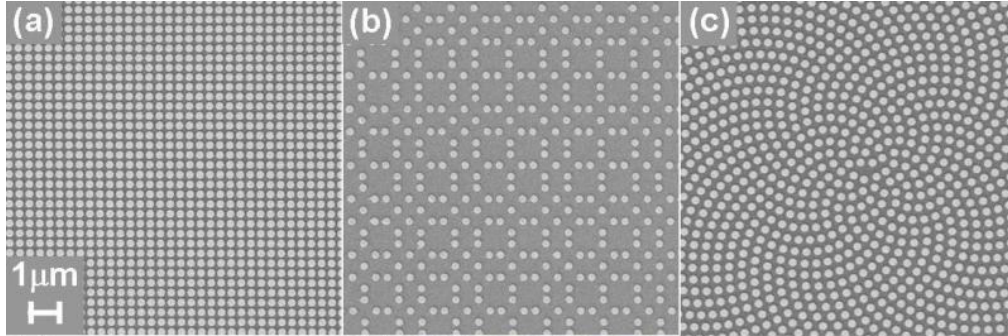


Fig. 1. SEM micrographs of periodic (a), Fibonacci (b) and GA spiral (c) arrays of 200nm-diameter cylindrical gold nanoparticles with a particle separation of 60 nm.

### 3. Dark-field characterization

Prior to SHG experiments, we characterize the linear behavior of each fabricated array by measuring their dark-field scattering spectra. We use a broadband halogen lamp, a 50x objective with 0.5 NA and a fiber coupled CCD spectrometer (Ocean Optics QE65000). Dark-field scattering spectra are plotted in Fig. 2 for the three array geometries and for different interparticle separations $L$. In periodic arrays (Fig. 2(a)) we notice that for values of $L$ larger than the particle size (yellow, cyan, magenta and blue curves) the scattering resonance peak blue-shifts when $L$ decreases due to photonic (*i.e.*, diffractive) coupling among the nanoparticles. Conversely, for values of $L$ comparable to the particle size (green and red curves), the quasi-static near-field interaction among closely spaced particles prevails over the photonic one, and a broad resonance towards the near-infrared is observed. We refer to this regime as plasmonic coupling. In contrast, Fibonacci arrays (Fig. 2(b)) exhibit a broader scattering peak around 800 nm with no remarkable shift as the interparticle separation $L$ is varied. This scattering behavior is consistent with the inhomogeneous spatial distribution of nanoparticle dimers in Fibonacci arrays, that leads to a more incoherent scattering response largely insensitive to $L$ [21–24]. Interestingly, the scattering behavior of the GA spiral arrays (Fig. 2(c)) is similar to the one of periodic structures. In particular, the GA spiral array features well distinct photonic and plasmonic resonances, similar to periodic arrays. In fact it has recently been shown that these structures display local order, captured by oscillations in the particles radial correlation function and by a well-defined scattering ring in Fourier space [26].

In Fig. 2(d) we show the behavior of the scattered intensity at 780 nm, later utilized as the pump wavelength in the pulsed SHG experiments, versus the interparticle separation for the different array geometries. In the case of periodic arrays (red squares), the highest value of the scattered intensity occurs at $L = 611$ nm, corresponding to a center-to-center interparticle distance of 811 nm. This resonance may be associated with surface plasmon coupling with the grating periodicity [30,31]. GA spiral arrays (blue circles) show a trend similar to that observed for periodic arrays. On the contrary, the linear scattering from Fibonacci arrays (green triangles) is almost insensitive to variations in $L$, consistently with its more incoherent

nature. The increase in scattering signal when decreasing the interparticle separations in a Fibonacci arrays reflects the increase in the particle number.
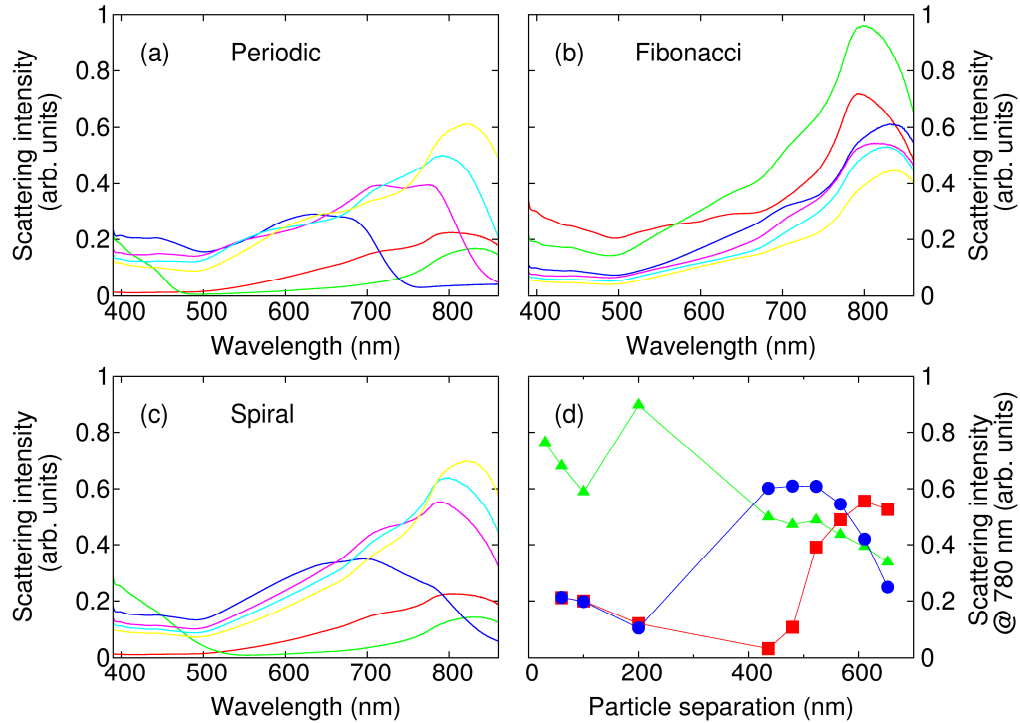


Fig. 2. Dark-field scattering intensity spectra for periodic (a), Fibonacci (b) and GA spiral (c) arrays with different interparticle separation $L$: 60 nm (red), 200 nm (green), 436 nm (blue), 523 nm (magenta), 567 nm (cyan), 653 nm (yellow). (d) Dark-field scattering intensity at $\lambda$ = 780 nm for periodic (red squares), Fibonacci (green triangles) and GA Spiral (blue circles) arrays versus $L$.

## 4. Pump power dependence

The SHG from the three array geometries is studied by exciting the samples at 780 nm with a femtosecond Ti:Sapphire pulsed laser (Mai Tai HP, Spectra Physics), with a pulse width of 120 fs and repetition rate of 80 MHz, which is reduced to 10 MHz by an electro-optic pulse picker (Conoptics 360-80l). The laser beam is filtered by a 700 nm long-pass filter and has an average power of 40 mW. We utilize the specular reflection configuration shown schematically in Fig. 3(a). The excitation is obliquely incident on the sample surface at an angle $\varphi$ = 45° and the reflected SHG signal is collected. The beam is focused onto the array by an 85 mm focal length spherical lens. The signal is collected through a 50x microscope objective with a numerical aperture NA = 0.5 and is detected by a Newport 77348 photomultiplier tube (PMT) after passing through a monochromator (Cornerstone 260 1/4 m Triple Grating, Ruled, 1200 l/mm, 500nm Blaze, 280-1600nm Primar). A lock-in amplifier (Oriel Merlin) extracts the signal modulated by a mechanical chopper. The collected signal is filtered by a 650 nm short-pass filter before the PMT in order to reduce the intensity of the pump component at the detector.

We measure the intensity of the collected signal both at the pump wavelength and at the SHG wavelength (*i.e.*, 390 nm). Figure 3(b) shows representative SHG spectra from arrays with interparticle separation $L$ = 60 nm, as a function of the pump power density W normalized to the maximum pump power ($W_{max}$). We operate with $W_{max} \approx 2$ kWcm$^{-2}$ in order to preserve the NPs structure and to avoid sample damaging. Figures 3(c) and 3(d) show the intensity of the collected signals at the pump and at the SHG wavelength, respectively, versus

the pump power intensity for periodic (red squares), Fibonacci (green triangles) and GA spiral (blue circles) arrays with interparticle separation of 60 nm. A linear fit in a log-log scale indicates a slope ≈ 1 for the scaling of the fundamental signal and ≈ 1.8 scaling for the SHG signal. A quadratic dependence of the SHG signal on the pump power is the hallmark of a second order nonlinear process. We attribute the small discrepancy from the expected quadratic dependence to thermal effects in gold NPs well below the melting point [16].
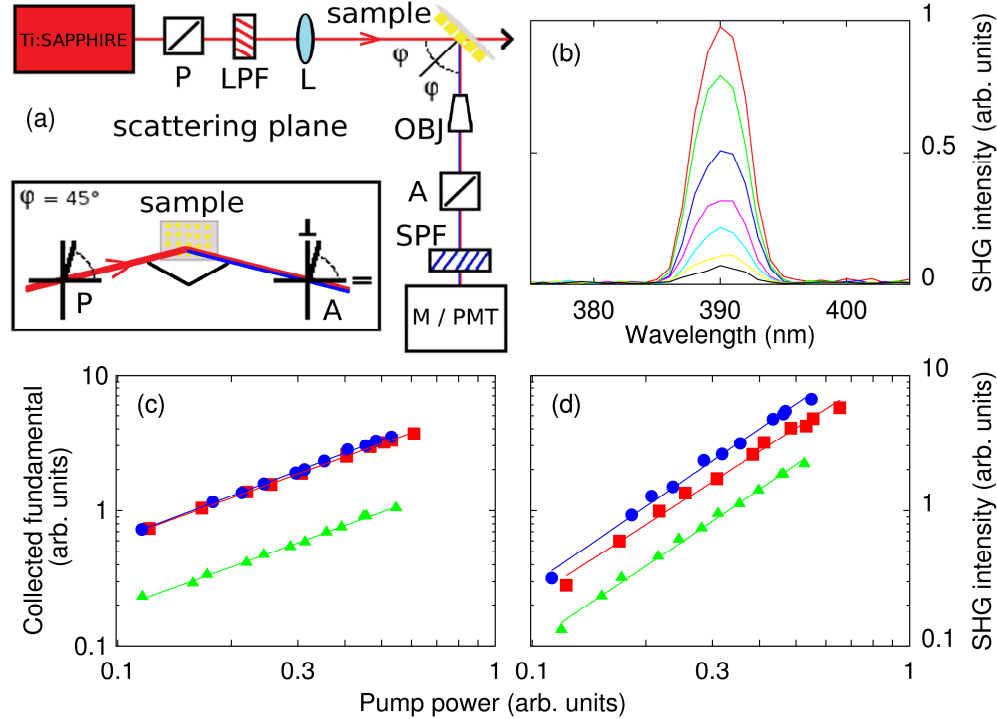


Fig. 3. (a) Schematics of the excitation-collection configuration; (b) spectra of SHG signals from arrays with interparticle separation of 60 nm, for several pump power densities W/W$_{max}$: 1 (red), 0.821 (green), 0.654 (blue), 0.525 (magenta), 0.402 (cyan), 0.290 (yellow), 0.213 (black); (c) collected signals at pump wavelength ($\lambda$ = 780 nm) and (d) SHG wavelength ($\lambda$ = 390 nm) versus pump power intensity for periodic (red squares), Fibonacci (green triangles) and GA spiral (blue circles) arrays with interparticle separation of 60 nm. Scales are logarithmic.

## 5. Polarization dependence of the SHG

The contribution of multipolar sources to SHG can be recognized by their far-field emission. In what follows, we investigate the polarization properties of the second harmonic radiation with the aim of demonstrating its multipolar nature for the three planar array geometries [10,32–36]. It was recently predicted that multipolar SHG signal is more sensitive than the fundamental one for sensing applications [35]. We consider the components of the collected signal that are parallel and orthogonal to the scattering plane, defined by the directions of excitation and collection (inset of Fig. 3(a)). We measure the intensities of the two polarization components at the SHG wavelength as a function of the input polarization angle of the pump beam through a polarizer/analyzer pair. A zero angle corresponds to a polarization parallel to the scattering plane. Following Brevet *et al.* [32–34], the experimental data are fitted using Eq. (1), where *a*, *b* and *c* are real parameters.

$$I(\gamma) = a\cos^4(\gamma) + b\cos^2(\gamma)\sin^2(\gamma) + c\sin^4(\gamma) \tag{1}$$
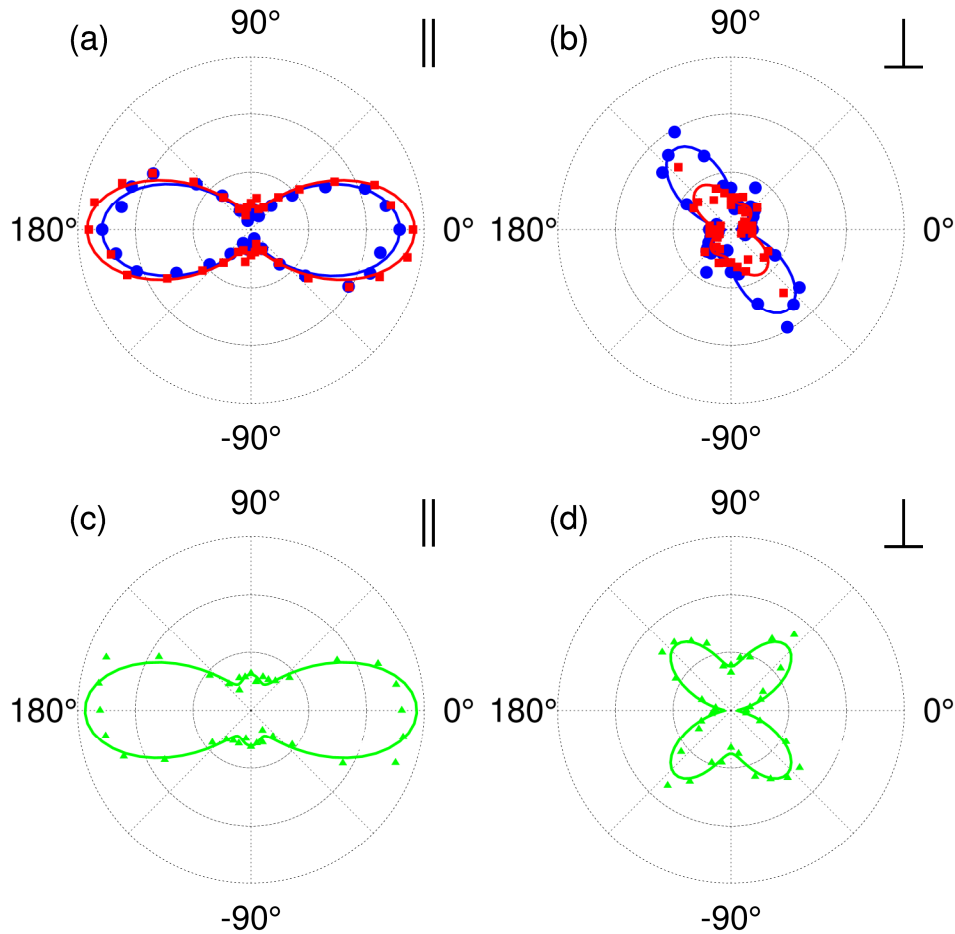
Fig. 4. Intensity of the radiated SHG parallel (a) and orthogonal (b) components for periodic (red) and spiral (blue) arrays; intensity of the radiated SHG parallel (c) and orthogonal (d) components for the Fibonacci array (green). Experimental data is with scattered symbols, least-squares fit is with continuous lines. The intensities in the plots of panel (a) have been reduced of the factor 11/4 for the sake of clearness.

In Fig. 4(a) and 4(b) we show the intensities of the parallel and orthogonal components for the SHG signal of periodic and GA spiral arrays, while Fig. 4(c) and 4(d) display the results of the Fibonacci array. We notice in Fig. 4(a) and 4(c) that the polar plots of each parallel component do not exhibit the typical patterns of a dipolar source, which is insensitive to the angle of polarization of the pump [10,32–34]. This can be more clearly appreciated by the fact that when using $2a = 2c = b$ in Eq. (1), as required for the parallel component of a dipolar source, we cannot fit the experimental data in Fig. 4. Hence, higher order multipolar contributions need to be considered due to symmetry breaking and retardation effects, which are particularly relevant for non-spherical particles in the investigated size regime.

On the other hand, a quadrupolar SHG behavior is displayed by the orthogonal component for the Fibonacci array in Fig. 4(d), which can only be fitted when $a, c \ll b$. This is expected since for a pure quadrupolar source $a = c = 0$. To the best of our knowledge, this is the first time that a quadrupolar radiation patterns has been directly measured in the SHG signal from planar arrays of metal NPs. The polar plot in Fig. 4(d) is similar to the behavior of the orthogonal component of the SHG measured in systems of non-interacting spherical nanoparticles [10,32–34]. On the contrary, the photonic interactions among NPs radically

modify the SHG radiated from periodic and GA spiral arrays. For these array geometries, the polarization patterns of the orthogonal components (Fig. 4(b)) are different from a pure quadrupole, and high order multipolar SHG emission is observed [33,34]. In fact, Eq. (1) does not fit the experimental data for any value of the parameters, and a modified version must be introduced as in Ref. [32,33]:

$$I(\gamma) = a\cos^4(\gamma) + b\cos^2(\gamma)\sin^2(\gamma) + c\sin^4(\gamma) + d\cos^3(\gamma)\sin(\gamma) + e\cos(\gamma)\sin^3(\gamma). \quad (2)$$

The quadrupolar SHG polarization dependence displayed by Fibonacci quasi-periodic arrays with respect to periodic ones and GA spiral structures may reflect the different linear scattering behavior displayed at the fundamental frequency, as discussed in Section 3.

The values of the parameters *a*, *b, c, d* and *e* utilized to fit the experimental data are displayed in Table 1.

**Table 1. Fitting Parameters**

| Array geometry | SHG component | a | b | c | d | e |
|---|---|---|---|---|---|---|
| Periodic | parallel | 0.210 | 0.622 | 2.371 | - | - |
| Periodic | orthogonal | 0.228 | 1.219 | 0.035 | 0.587 | 0.040 |
| Fibonacci | parallel | 0.206 | −0.025 | 0.957 | - | - |
| Fibonacci | orthogonal | 0.252 | 1.642 | 0.038 | - | - |
| GA spiral | parallel | 0.371 | 0.501 | 2.610 | - | - |
| GA spiral | orthogonal | 0.184 | 0.660 | 0.073 | 0.181 | 0.095 |

## 6. Dependence on the interparticle separation

The intensity of the SHG signal is plotted as a function of the interparticle separation *L* for all the arrays in Fig. 5(a). A clear dependence of the SHG signal on the interparticle distance *L* is observed, and the largest *L* produces the weakest SHG response for each array geometry.

Moreover, we notice that GA spirals give rise to the strongest SHG signals for all the investigated values of interparticle separations. On the other hand, for Fibonacci arrays the SHG is the lowest for all separations. This can be attributed to the lower particle filling fraction of Fibonacci arrays. The variation in the particle filling fraction of all the arrays as a function of the interparticle separation is shown in the inset of Fig. 5(a). Furthermore, we notice that the superior performances of GA spirals over periodic arrays cannot simply be explained by the difference in particle filling fractions, as these are comparable across the investigated range of separations. Therefore, we attribute the enhanced SHG to the asymmetric spatial near-field distribution in GA spiral arrays, which is a consequence of their distinctive spiral aperiodic order. The importance of the near-field intensity distribution at the pump wavelength for the SHG optimization was already pointed out by Canfield et al. in the case of asymmetric metal nanoparticles [18].
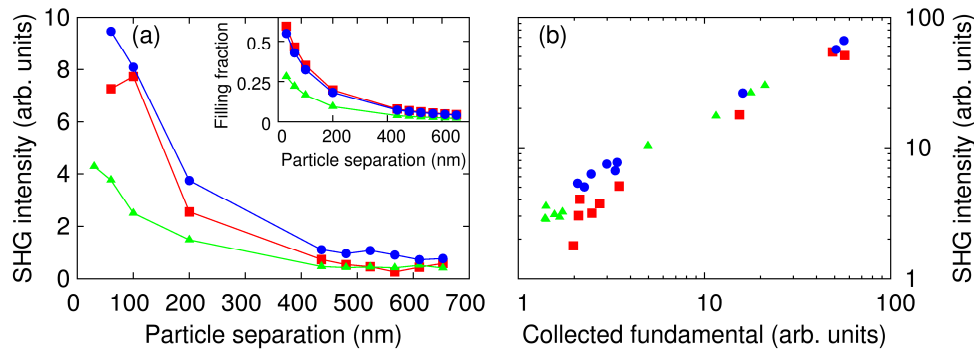


Fig. 5. (a) Intensity of the collected SHG signal as a function of the interparticle separation *L*, for periodic (red squares), Fibonacci (green triangles) and GA Spiral (blue circles) arrays; (a inset) Filling fraction of gold for periodic (red squares), Fibonacci (green triangles) and GA Spiral (blue circles) arrays; (b) correlation diagram between SHG and pump collected signals.

In Fig. 5(b) we show a correlation between the intensities of the SHG signal and of the scattered pump at 780 nm. A direct dependence of SHG signal on the fundamental is demonstrated, showing that the SHG is mainly driven by the optical behavior of the NP arrays at the pump frequency. In general, the SHG process depends also on the NP array field distribution at the harmonic frequency, but in this case the strong absorption of gold at the SHG frequency makes this dependence negligible. In order to better understand the role of the asymmetry of the spatial distributions of the pump field over the NPs, we show in Fig. 6 the calculated near-field patterns at 780 nm, obtained by the Generalized Mie Theory (GMT) [37]. The pump fields are calculated in the plane of the arrays for all the array geometries and for two particle separations (60 nm, 611 nm) characteristic of plasmonic near-field coupling and photonic coupling, respectively.

Figure 6(a) and 6(c) show that periodic arrays display a very regular distribution of near-field around each NP, and the local field intensity is reduced as the NPs are separated. Moreover, we notice that the field is strongly oriented along the direction of polarization of the pump beam. The highly symmetric nature of the near-field pump distribution in periodic plasmonic arrays reduces the SHG signal due to destructive interference [4,13]. In Fig. 6(b) and 6d, we show the near-field distributions in GA spiral arrays for the photonic and plasmonic coupling regimes, respectively. The GA spiral geometry couples all the particles in the array but, differently from periodic structures, a very asymmetric near-field distribution results from the distinctive aperiodic order. This asymmetry of the pump fields in the GA spirals prevents destructive interference effects in the SHG for all interparticle separations, resulting in a stronger SHG signal, as we experimentally demonstrated over a large range of particle separations.
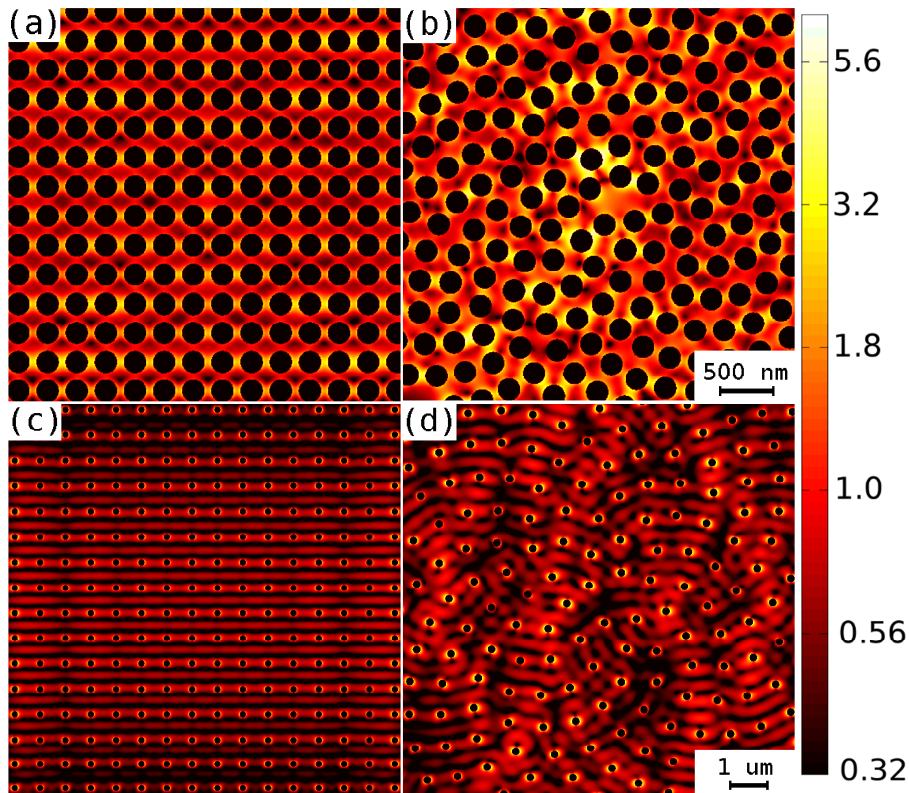


Fig. 6. Near-field distribution at the pump frequency over periodic (a) and GA spiral (b) arrays with interparticle separation $L = 60$ nm. Near-field distribution at the fundamental frequency over periodic (c) and GA spiral (d) arrays with interparticle separation $L = 611$ nm. All the near-field maps are plotted in logscale.

## 7. Conclusion

We studied the role of the planar array geometry on the SHG from gold NPs. In particular we investigated periodic arrays, quasi-periodic and aperiodic arrays. We demonstrated quadrupolar SHG from planar arrays of metallic NPs and its tunability with the array geometry. Moreover, we demonstrated more intense SHG in aperiodic GA spiral geometry compared to the periodic one, and over a large range of particle separations. We explain this behavior by the asymmetric near-field distribution of aperiodic GA spiral at the pump wavelength. These results are important for the development of novel optical elements for nonlinear nanophotonics applications, such as switchers, frequency converters and nonlinear optical sensors on a planar chip.

## Acknowledgments